Check for updates

Robust heart rate monitoring by a wearable stethoscope based on signal processing

Jingyi Xu,[a] Wenru Zeng,[b] Chao Zhao, (iD) *[a] Jiayi Tong[c] and Hong Liu (iD) [a]

Heart rate monitoring is of great importance for the early diagnosis of cardiovascular diseases or the assessment of mental status. The most popular methods are electrocardiography (ECG) on the thorax in the hospital and photoplethysmography (PPG) on the dorsum manus in daily life. In this work inspired by auscultation, a wearable stethoscope with biocompatible adhesives was designed and assembled along with an application for robust heart rate monitoring. The geometry of the adhesives was firstly optimized, and the device was compared to PPG with several advantages. Then it was demonstrated on different arteries of the body. Algorithms were performed to make our device robust under some motion artifacts or environmental noise. At last, the accuracy of our device for continuous heart rate monitoring compared with ECG as the gold standard indicates that our system could potentially provide a new wearable technology, which could help realize early diagnosis of cardiovascular diseases or mental illness related to abnormal heart rate within different time scales.

Introduction

Cardiovascular diseases (CVDs) have been the leading cause of death, resulting in more than 19 million deaths worldwide in 2020.[1] In South Asia, 35.5% of deaths are caused by CVDs, ranking the highest in the world.[2] The most common CVD is arrhythmia, which is mainly atrial fibrillation (AF) where the heart beats irregularly and faster than normal. Despite the high mortality of CVDs, 90% can be prevented through early detection of abnormal heart rate.[3] Heart rate (HR) can be measured by detecting the pulse frequency of arteries, as every ventricular contraction will transmit a pulse in blood vessels normally, and its monitoring is an effective way of non-invasive cardiovascular health assessment. An increase of resting HR and lagged responses of exercising HR were supposed to reflect the severity of CVDs.[4,5] Not only is the irregular heart rate of CVDs in a short time segment (several seconds) meaningful, the heart rate in the whole continuous monitoring time period (tens of minutes) is also important, such as for the early diagnosis of mental illness such as depression and anxiety. People with mental illness are prone to have a smaller entropy of HR compared to normal ones, as the sympathetic and parasympathetic nervous system cannot modulate HR effectively. Nevertheless, clinically the patients

are required to wear a Holter monitor for 24 hours or longer, so as to find HR irregularities for CVDs or mental illness. It is bulky and limits the application scenarios for early diagnosis of related diseases. Thus, the long-term monitoring of HR *via* wearable technologies is vital with sensors attached to the epidermis (fingertip, neck, wrist, *etc.*) near the artery, and becomes a hot topic in the diagnosis community.

ECG is widely recognized as the gold standard for HR monitoring, while it is hard to make it wearable on exposed skin. Compared to ECG, wearable pulse wave detections were commonly based on optoelectric,[6-10] bioimpedance,[11-15] ultrasonic,[16] and mechanoelectric techniques[17-19] to obtain PPG, impedance plethysmogram (IPG), ultrasonogram (USG), pulse waveforms (PW), *etc.* Nevertheless, the optoelectric method usually demands an additional 5 V power for the LED, which makes the device power inefficient, and the power detector could be easily interfered by ambient light in the environment. Bioimpedance measurement requires an additional electrical signal of several thousand Hz for stimulation and the impedance change caused by pulses is only several mΩ, which needs a complicated backend readout electric circuit. Ultrasonic techniques are harmful for tissues during long term monitoring, and not recommended for usage longer than 30 minutes, not to mention the complex structural design of the piezoelectric sensor array. As a mechanical wave, the pulse wave can be recognized by piezoelectric, piezoresistive or inertial sensors. The advantage of the mechanoelectric method compared to the other three is that it requires no optical, electrical, or ultrasonic stimulation on the body, and this passive sensing makes it

[a] *State Key Laboratory of Bioelectronics, School of Biological Science and Medical Engineering, Southeast University, Nanjing 210096, China.*
E-mail: czhao@seu.edu.cn
[b] *Nanjing Drum Tower Hospital, Nanjing 210000, China*
[c] *Zhongda Hospital, Southeast University, Nanjing 210096, China*

power efficient, and suitable for ultralong continuous monitoring. We previously reported robust heart rate monitoring by a single accelerometer[18] and patterned liquid metal sensors.[17] However, they could hardly detect pulse waves on arteries embedded some distance away from the skin. Auscultation is another mechanoelectric method that could sense the sound wave deep inside the body, and was recently engineered to be attached to the chest for monitoring heart beating and lung sound.[20]

Besides the sensing methods, the interface between a wearable device and human skin influences the wearing comfortability, biocompatibility, and signal quality. A firm adhesion between the skin and the device will increase the signal to noise ratio (SNR) due to the apparent damping of motion artifacts and has been paid more attention in recent years.[8,9,21–23] Soft biocompatible materials (silicone, medical tapes, hydrogel, etc.) are commonly used as the adhesive layer for their excellent softness and stretchability, while forming conformal interfaces between the device and skin.[24–26] Liu et al. synthesized a nonyl and glycerol-modified polyvinyl alcohol with high stretchability (598%), low elastic modulus (5 MPa), and high adhesion (6.33 kPa), which performs better than non-adhesive PDMS during electrophysiological signal monitoring.[27] Liu et al. fabricated a micro-structured, natural silk fibroin protein-based adhesive as a strain sensor with excellent conformal and tunable adhesion on skin surfaces which will not cause significant pain when stripped.[28]

In addition to the device hardware and biocompatible adhesives, an algorithm for denoising was proven to boost the HR estimation accuracy, especially as the wearable pulse wave signal is vulnerable to environmental noise and motion artifacts (MA). Frequency domain filtering and signal decomposition are commonly used to deal with the challenge. Alessandra et al. filtered the disturbed PPG by singular value decomposition (SVD) and discrete Fourier transform (DFT), and then Kalman smoothing was utilized for further optimization. The calculated HR is equivalent to the ECG reference value within a few minutes.[29] Motin et al. adopted a decomposition strategy to extract HR from PPG signals by empirical mode decomposition (EMD) and principal component analysis (PCA) with RMS error less than 1 bpm.[30] Besides noise removal, Chung et al. proposed a HR estimation method based on a finite state machine (FSM) and crest factor to improve the accuracy of HR by selectively extracting PPG signals with high SNR.[31] Previously, we also compared several signal decomposition methods on monitoring HR by accelerometers, and the device was demonstrated to meet the accuracy needed for medical usage based on the guideline of ANSI/AAMI EC13.[32]

Here, inspired by auscultation in the hospital, which has been widely applied in health monitoring and disease diagnosis, another passive sensing by a microphone IC chip with an integrated microelectromechanical system (MEMS) is introduced and demonstrated with specific advantages, such as small size, high SNR and flat wideband frequency response.[33] The novel wearable small-scale electronic

stethoscope (WSES) system could record pulse sound (PS) for HR monitoring with high SNR and robustness. A user-friendly mobile device application was also developed to record and display pulse waves wirelessly. With signal processing, our device could still monitor HR under environmental noise and motion artifacts. This work showed that with an optimized device, it could be attached to several different arteries on the body, and monitor HR for a long time for future applications, such as diagnosis of CVDs or mental illness.

Methods

Hardware and device assembly

Fig. 1 exhibits the design and photo of the hardware and biocompatible adhesives, schematics and photo of monitoring HR by our device. As shown in Fig. 1a, the heart contracts to supply blood to all round the body, causing periodic changes in the diameter of arteries. The expansion and recovery of vessels generates mechanical waves called pulse sound, which can be detected by a microphone (MIC). Pulse sound goes through the tissue and air, leading to the vibration of the sensing components in the IC chip. The inner converter converts the mechanical energy into an electrical signal which was captured. The signal is then acquired and sent out wirelessly by Bluetooth, and received by an application (APP) specially developed for the real-time display and in-memory storage of the pulse sound data. After transferring off-line pulse wave data from the smartphone to the computer, signal processing algorithms based on wavelet decomposition, peak detection and fusion, and Kalman filtering are employed for continuous HR monitoring (Fig. 1b). Fig. 1c shows the 3D view of the detailed structure and components of the WSES, which mainly includes a circuit board with an IC, electronic components and biocompatible adhesives. The hardware consists of (1) a MEMS MIC (ICS-43432, InvenSense), with 3.5 mm × 2.6 mm
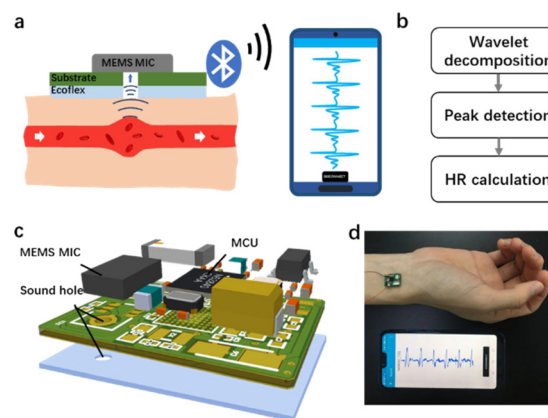

Fig. 1 Design and demonstration of the WSES. (a) Schematics of HR monitoring by our device. (b) Flow chart of signal processing. (c) Design of the device with a PCB and adhesives. (d) Photo of the WSES monitoring HR.

size, for pulse sound sensing, (2) a microcontroller unit (MCU) (nRF52840, Nordic Semiconductor), with 3.5 mm × 3.6 mm size, for receiving data from the MIC and transmitting it to the mobile phone *via* Bluetooth low-energy (BLE) protocols, (3) a low dropout regulator (MIC5219, Microchip), with 2.9 mm × 1.6 mm size for providing stable power voltage for the system, and (4) the relating resistances, capacitances and antenna. The whole hardware is 14.8 mm ×11.2 mm in size. The device works at a sampling rate of 2.4 kHz, which is enough to record pulse sound without distortion. It can be powered by a 3.7 V, 1000 mAh lithium battery and works persistently for more than 160 hours. The biocompatible adhesives are Ecoflex films with a sound hole at the same position as the MIC. The sound transfers from the blood vessel to the air gap and the adhesives are able to concentrate the sound and remove some environmental noise. The real time HR monitoring by our device is shown in Fig. 1d. The whole device is compact and wearable, and is capable of being attached on most arteries of the body for pulse sound wave detection.

Adhesive preparation and optimization

The adhesion layer between the circuit board and human skin is of great importance for pulse sound detection, which is capable of isolating the external environment sound partly and ensuring the MIC adhering to the skin totally to increase the SNR. In this study, Ecoflex (0030) film was utilized as the biocompatible adhesive. It is a kind of silicone with good biocompatibility and conformability, and has been applied in several works to detect physiological signals.[20,33] A series of Ecoflex films with different heights were fabricated and studied to explore the influence of thickness on the SNR. In addition, the size of the sound hole was optimized to determine the acoustic impedance and filtering ability of the hole.[34] The pulse wave signal quality was greatly influenced by the resistance of laminar flow in the sound hole, which can be calculated by the Hagen–Poiseuille equation:

$$R_h = 8 \frac{\eta \cdot l}{\pi \cdot r^4}$$

where η is the viscosity of the air, and l and r are the length and radius of the hole, respectively. The performance of different Ecoflex films was quantified by SNR:

$$SNR = 10 \lg \frac{\sum S_{fil}^2}{\sum (S_{ori} - S_{fil})^2}$$

where S_{fil} is the output of a 50 Hz low-pass filter to remove noise, which is considered as the clear pulse sound signal, and S_{ori} is the original signal collected by the WSES.

The detailed experimental procedure is as follows:

(1) Mix the part A and part B of Ecoflex at a 1 : 1 ratio and pour the mixture into the mold to make five films of different thicknesses (0.2, 0.5, 0.8, 1.2 and 1.5 mm).

(2) Drill the film with a borer to leave a hole of diameter of 1 mm, which is the same as the MIC's sound hole.

(3) Stick these films under the circuit board, respectively, with the holes of the MIC and adhesives aligned.

(4) Put the assembled device on the wrist for pulse wave detection and SNR calculation. In order to assure the position consistency, a marker pen was used to draw an outline to make sure that the sensor was attached at the same site. Choose the thickness of the film with a maximum SNR for the next experiment.

(5) Drill five films at the optimized thickness with different sizes of borers (0.5, 0.8, 1, 1.2, and 1.5 mm). Repeat steps (3) and (4) to determine the optimal sound hole size with the highest SNR.

Signal denoising, peak detection and HR calculation

In order to obtain accurate HR values, the original waveforms will undergo a set of signal processing algorithms shown in Fig. 2.

Firstly, signal denoising is operated. The pulse wave signal could be interfered by environmental noise and motion artifacts, which usually have high amplitude and overlap with pulse waves in the frequency domain. The denoising method is critical for improving SNR. We tested several noise reduction algorithms (wavelet decomposition, variable mode decomposition and Fourier decomposition) and found that wavelet analysis is the most suitable for the low-pass filtering of pulse sound. A 6-layer wavelet decomposition of the pulse wave is done by the 'db3' wavelet, which resembles the signal of the pulse wave. We took the approximate coefficient reconstruction results of the sixth layer (a6) as the filtered signal, which contains nearly no high frequency noise in the waveform.

Next, a peak detection method is applied. The high frequency part of noise is mostly removed by the wavelet decomposition. However, some motion artifacts which have the same frequency range as pulse waves are not removed. Considering that a pulse wave recorded by the MIC consists of both positive and negative peaks, which have analogous absolute values, while the motion artifacts show unbalanced distribution near the baseline, we labelled both positive and negative peaks of the pulse waves and performed peak fusion
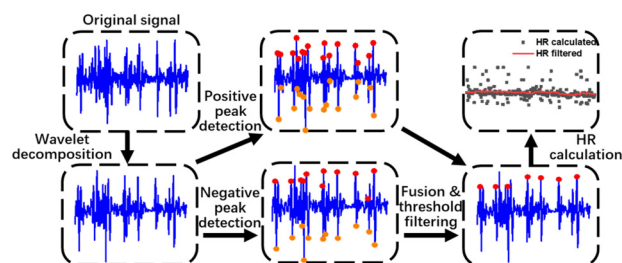

Fig. 2 Workflow of signal processing, including wavelet decomposition, positive and negative peak detection, fusion and threshold filtering and HR estimation.

to boost the accuracy of the peak detection. The specific steps are as follows:

(1) Set a 5 s long time window to segment the signal. In each time segment, a 15 Hz low-pass filter is firstly employed to eliminate outliers. Find the maximum and minimum of the filtered signal in a time segment and record them as y_{max} and y_{min}.

(2) Search for the positive peaks in a window of 200 data points. The peaks that are smaller than $0.5 \times y_{max}$ are discarded, with the remaining peaks recorded. Depending on the initial direction of the pulse wave signal, we decide to search for negative peaks before or after the positive peaks in a window of 300 data points. Then, seek the nearest negative peaks in a window of 60 data points within those 300 data points. All the positive and negative peaks identified are recorded.

(3) Similar to in step (2), the negative peaks are identified and recorded.

(4) Merge both positive and negative peaks together. If the distance between two adjacent positive and negative peaks is smaller than $F_s \times 60/150$, where F_s is the sampling rate, the one with the smaller amplitude difference is discarded, and the remaining one will be marked as a pulse beat.

(5) Finally, calculate the pulse wave interval time to get HR values. Then, outliers are smoothed by a Kalman filter in MATLAB with system covariance at 1 and observation covariance at 100.

Miscellaneous

After assembling the hardware with optimized adhesives, the pulse sound from our device on the wrist was compared with PPG, obtained from the thumb at the same side of the wrist using a commercial evaluation system (MAX86150EVSYS, Maxim Integrated). For comparison with HR monitoring using ECG as the gold standard, an ECG chest belt (Polar H10, Polar Electro) was chosen to estimate the performance of our device. For demonstration of versatile HR sensing on different arteries, we collected the pulse waves from the wrist, elbow, neck and temple. All participants provided their signed informed consent and the study was approved by the Ethical Committee of the Southeast University. The data were acquired according to the guidelines of the University's Ethical Committee.

Results and discussion

Biocompatible adhesive thickness and sound hole size

Firstly, the thickness and sound hole diameter of the biocompatible adhesives were optimized. The performance of different heights of the adhesion layer and sound hole diameter is shown in Fig. 3. Thin adhesives will decrease the resistance theoretically, but the hard electronic device will not adhere conformally to the skin if the adhesives are too thin. Ecoflex films with heights at 200, 500, 800, 1200 and 1500 μm were fabricated with a hole of 1000 μm and attached to the artery on the wrist for HR monitoring. SNR of the pulse wave is calculated and shown in Fig. 3a. Indeed,
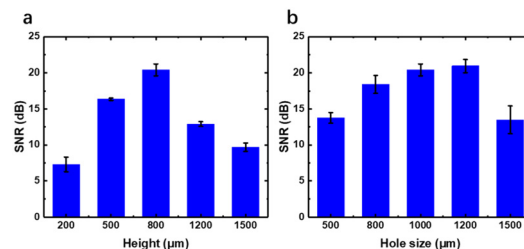

Fig. 3 Parameter optimization of the Ecoflex adhesion layer. (a) SNR of different heights of adhesives at 200, 500, 800, 1200, and 1500 μm. (b) SNR of different diameters of the sound hole at 500, 800, 1000, 1200, and 1500 μm.

our result showed that the thickness at a height of 800 μm performs best with a SNR at 20, while the smallest SNR is only about 7 when the thickness is 200 μm.

Then, the diameter of the sound hole was adjusted. As the diameter of the sound hole of the MEMS MIC was fixed at 1 mm, we fabricated Ecoflex films with the height at 800 μm and hole size at 500, 800, 1000, 1200 and 1500 μm. The SNR is shown in Fig. 3b, from which the hole a bit larger (1200 μm) than the MIC sound hole is the best choice, as it may help in collecting more area of pulse wave resonance. However, the SNR dropped rapidly if the size turned larger at 1500 μm for energy leakage and bad sound collection, with the same performance with the hole size at 500 μm. So, all the following experiments were performed using an Ecoflex film optimized with the thickness at 800 μm and hole size at 1200 μm. The adhesive layer can be reused at least 15 times. Clean the layer with alcohol if necessary.

Pulse sound waveforms

Then, our optimized device was attached to the artery on the wrist, and compared with PPG on the finger at the same side (Fig. 4a). It can be seen that the two signals have basically the same vibration frequency during 5 seconds. Averaging the waves of each pulsation, the profile of three peaks of pulse sound is similar to that of PPG (Fig. 4b), which is the typical pulse wave signal in a cardiac cycle. It contains an evident main peak followed by two shorter sub-peaks marked
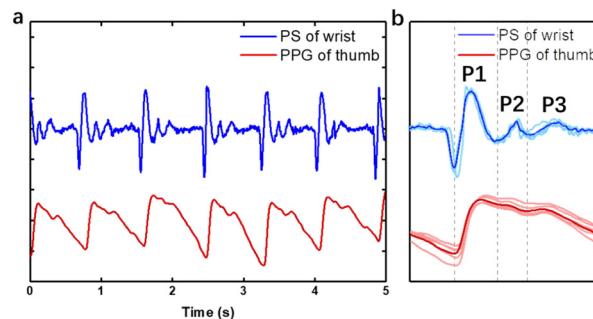

Fig. 4 Arterial PS wave response *vs.* PPG. (a) Wrist PS wave and thumb PPG signals in 5 seconds. (b) A typical averaged PS wave with an evident main peak P1 followed by two shorter sub-peaks P2 and P3.

as P1, P2 and P3, which represent the peaks of advancing wave, reflected wave and dicrotic wave, respectively. The three waves fluctuate around zero and repeat periodically when resting. Unlike ECG or PPG, the pulse sound signal will not be disturbed by baseline drift according to the amplitude symmetry of mechanical wave, which requires a simpler signal processing algorithm favoring its application as a wearable device. The energy of the pulse wave is mostly distributed in the frequency band below 20 Hz and reaches the highest around 5 Hz after Fourier transform, which is below the range of frequency that can be heard by human ears (20–20 kHz) but captured by our device.

Wearing positions

Not like PPG which is mostly utilized on the finger or wrist, our device could be attached to several arteries on the body for HR monitoring. The pulse wave signals of the radial artery, brachial artery, carotid artery and temporal artery from the wrist, elbow, neck and temple were tested on a 23-year-old man and are shown in Fig. 5. The wave of the radial artery and temporal artery (Fig. 5a and c) is inverted with negative values of P1, P2 and P3, compared to the neck and elbow. It originated from the initial vibrating direction of the MEMS in the microphone chip which could be random, which does not affect HR evaluation. The reflected wave recorded from the brachial artery (Fig. 5d) is less conspicuous than others. There are oscillation patterns at the end of reflected wave of carotid pulse sound signal (Fig. 5b). The waveforms from these blood vessels vary from each other, showing different features in orientation, amplitude and peak profile. It originates from the body posture, peripheral tissues, the difference of the dimensions, stiffness and depth of blood vessels.[35] The pulse sound signal can provide more information about the artery by non-invasive monitoring. Some diseases like hypertension, arteriosclerosis and diabetes can be reflected in the pulse wave pattern.

Motion artifacts and environmental noise

For wearable devices, environmental noise and motion artifacts are ubiquitous and affect the sensing quality severely, especially when the device is worn near the hand. Here, experiments were performed to investigate the anti-interference capability of the WSES. We recorded the original pulse waves during clenching and opening the fist (Fig. 6a), moving the arm either horizontally (Fig. 6b) or vertically (Fig. 6c), talking and in white noise environment (Fig. 6d). On the figures, the positive peaks of every pulse using our algorithm were also labelled (Fig. 6). It can be seen that clenching or opening the first imposed little interference on the pulse wave signal from the wrist (Fig. 6a). However, the arm's motion will introduce substantial high noise floor to the signal (Fig. 6b and c), but it can be removed by our algorithms. As for talking or environmental noise, the pulse sound signal peaks will not be submerged even in a very noisy (70 dB) environment (Fig. 6d). The locations of peaks were detected based on the signal after signal processing and marked on the original signal. It was obvious on processed signals, but not obvious on the original ones with environmental noise (Fig. 6d). By visual inspection of the pulse waveform, the accuracy of signal peak detection was more than 96% with motion artifacts and 98% with environmental noise. All the results showed that the WSES for HR monitoring could robustly monitor HR in daily life.

Robust HR monitoring for 30 minutes

The device was not only tested for tens of seconds, but also demonstrated acceptable performance for tens of minutes, and thus could be applied in diagnosing cardiac heart rate irregularity or mental illness. In the long-time monitoring experiment, we attached our device on the temporal artery for wearing convenience and minimum motion artifacts. During a time of about 30 minutes, the subject was ordered to do some daily activities such as sitting, walking, working on a laptop, talking, shaking head, nodding and squatting
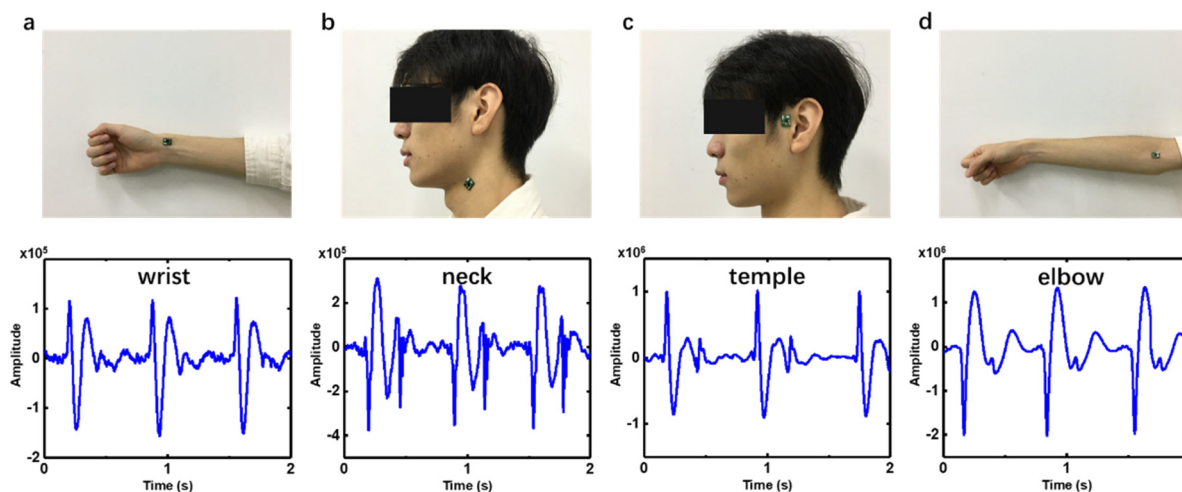

Fig. 5 Collecting PS signals from different arteries on the body, (a) wrist, (b) neck, (c) temple and (d) elbow.
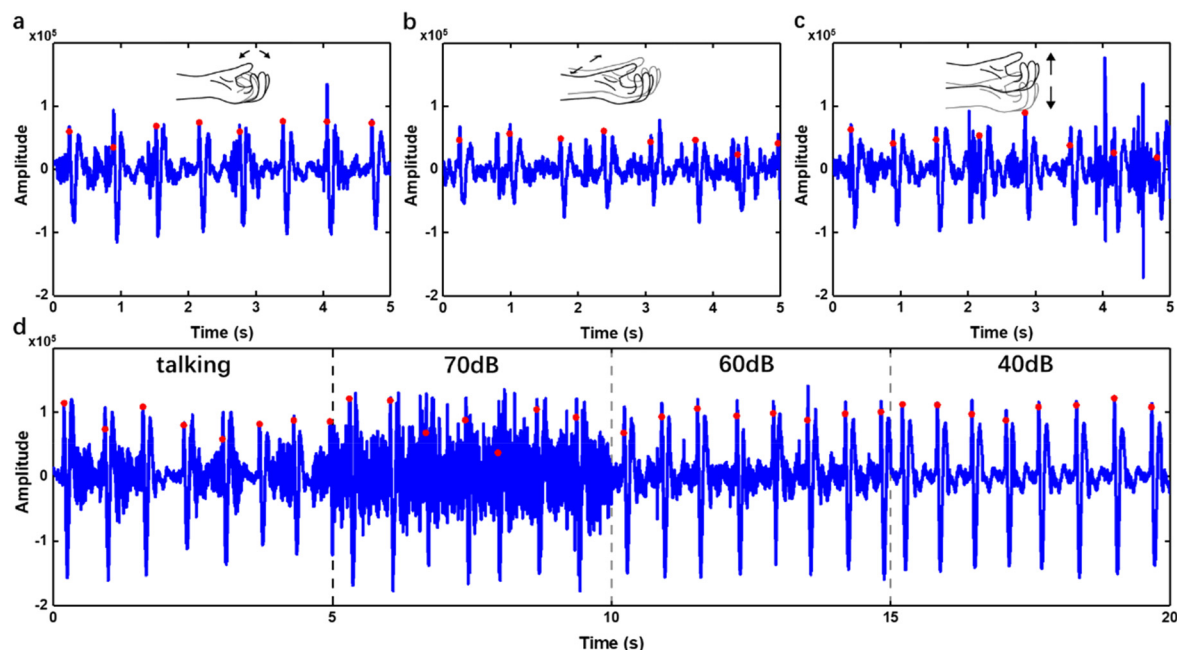
Fig. 6 The wrist PS wave and peak detection under motion artifacts or environmental noise: (a) clenching or opening the fist, (b) moving the arm horizontally, (c) moving the arm vertically, and (d) with people talking or white noise at 70 dB, 60 dB and 40 dB.
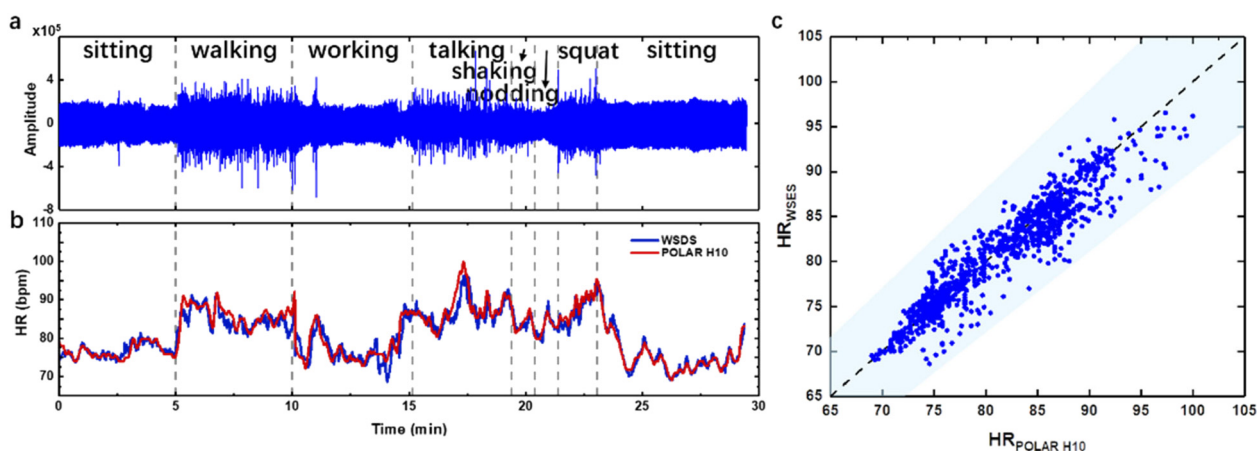

Fig. 7 HR monitoring for about 30 min during daily activities. (a) PS signal of 30 minutes. (b) HR estimation from the WSES and commercial Polar H10 as the gold standard. (c) Our device performed HR monitoring meeting clinical requirements.

(Fig. 7a). The subject also wore the commercial Polar H10, which is a HR monitoring system based on ECG. The raw pulse wave was shown with an estimated HR by our device and derived from Polar H10 (Fig. 7b). The discrepancy at 10 min and 13 min was from an unstable Bluetooth connection resulting in data loss, which caused the error in HR calculation. During the time course, the HR detection results of the WSES showed an excellent positive relationship with that recorded by the commercial device. Based on the guideline of ANSI/AAMI EC13, for a medical device, the estimated HR is recommended to be within ±10% or ±5 bpm, whichever is greater. These criteria refer to every individual HR estimation, and are quite difficult to meet for wearable sensors. In Fig. 7c, the shallowed area is defined by the

guideline, and our device already met the requirement, demonstrating that our device has great potential for medical application.

Nevertheless, several insights and limitations were identified. Firstly, different commercial or advanced biocompatible adhesives may be compared with Ecoflex, such as PDMS, Silbione substrate, 3M 2476P tape, 3M Tegaderm tape, 3M Micropore tape and others.[20] Also, the sound hole may be changed to other forms like sound hole arrays for acoustics. Secondly, further comparison between waveforms of pulse sound and PPG may be studied on more volunteers to correlate the three peaks (P1, P2, and P3) on different arteries of the body. The peak profile varies between different arteries, which may indicate other clinical significance.

Thirdly, more intensive motion artifacts during daily life, like jogging, running or bicycling, might be introduced to prove our system's robustness, with longer time such as several hours as the device is power efficient.

Conclusions

In this work, a novel WSES based on a microphone for non-invasive HR monitoring is developed. Attributed to the high performance of the MEMS microphone and optimized biocompatible adhesives, the system which is nearly the same size as a nail can record pulse wave signals with high SNR at more than 20 dB. The WSES exhibits various waveforms on different arteries, which may indicate some clinical characteristics of the arteries. It is proven that the outputs of HR from the WSES meet the medical standards and it can be used for daily heart rate monitoring. The developed WSES provides a new way of detecting pulse waves and will help in preventing cardiovascular diseases and mental illness.

Author contributions

C. Z. and H. L. conceived the research idea. J. X. performed experiments. J. X. analyzed the data. J. X. and C. Z. wrote the paper. All authors discussed the results and reviewed the manuscript.

Conflicts of interest

There are no conflicts to declare.

Acknowledgements

References

1 C. W. Tsao, A. W. Aday, Z. I. Almarzooq, A. Alonso, A. Z. Beaton, M. S. Bittencourt, A. K. Boehme, A. E. Buxton, A. P. Carson, Y. Commodore-Mensah, M. S. V. Elkind, K. R. Evenson, C. Eze-Nliam, J. F. Ferguson, G. Generoso, J. E. Ho, R. Kalani, S. S. Khan, B. M. Kissela, K. L. Knutson, D. A. Levine, T. T. Lewis, J. Liu, M. S. Loop, J. Ma, M. E. Mussolino, S. D. Navaneethan, A. M. Perak, R. Poudel, M. Rezk-Hanna, G. A. Roth, E. B. Schroeder, S. H. Shah, E. L. Thacker, L. B. VanWagner, S. S. Virani, J. H. Voecks, N. Y. Wang, K. Yaffe and S. S. Martin, *Circulation*, 2022, **145**, e153–e639.

2 P. Joseph, V. R. Kutty, V. Mohan, R. Kumar, P. Mony, K. Vijayakumar, S. Islam, R. Iqbal, K. Kazmi, O. Rahman, R. Yusuf, R. M. Anjana, I. Mohan, S. Rangarajan, R. Gupta and S. Yusuf, *Eur. Heart J.*, 2022, **43**, 2831–2840.

3 S. Chen, J. Qi, S. Fan, Z. Qiao, J. C. Yeo and C. T. Lim, *Adv. Healthcare Mater.*, 2021, **10**, 2100116.

4 D. Aune, A. Sen, B. ó'Hartaigh, I. Janszky, P. R. Romundstad, S. Tonstad and L. J. Vatten, *Nutr., Metab. Cardiovasc. Dis.*, 2017, **27**, 504–517.

5 S. Kurl, S. Y. Jae, A. Voutilainen, M. Hagnäs and J. A. Laukkanen, *Prog. Cardiovasc. Dis.*, 2021, **68**, 7–11.

6 J. Allen, *Physiol. Meas.*, 2007, **28**, R1–R39.

7 H. Lee, H. Chung, H. Ko and J. Lee, *IEEE Sens. J.*, 2018, **18**, 2983–2993.

8 H. Lee, H. Chung and J. Lee, *IEEE Sens. J.*, 2019, **19**, 1166–1175.

9 K. Xu, X. Jiang and W. Chen, *IEEE Sens. J.*, 2020, **20**, 3732–3744.

10 Z. Zhang, *IEEE Trans. Biomed. Eng.*, 2015, **62**, 1902–1910.

11 J. A. Berkebile, S. A. Mabrouk, V. G. Ganti, A. V. Srivatsa, J. A. Sanchez-Perez and O. T. Inan, *IEEE Trans. Biomed. Eng.*, 2022, **69**, 1909–1919.

12 T. Van Steenkiste, W. Groenendaal, P. Dreesen, S. Lee, S. Klerkx, R. de Francisco, D. Deschrijver and T. Dhaene, *IEEE J. Biomed. Health. Inform.*, 2020, **24**, 2589–2598.

13 K. Lee and H. J. Yoo, *IEEE Trans. Biomed. Circuits Syst.*, 2021, **15**, 1027–1038.

14 T. H. Huynh, R. Jafari and W. Y. Chung, *IEEE Trans. Biomed. Eng.*, 2019, **66**, 967–976.

15 D. Kireev, K. Sel, B. Ibrahim, N. Kumar, A. Akbari, R. Jafari and D. Akinwande, *Nat. Nanotechnol.*, 2022, **17**, 864–870.

16 C. Wang, X. Chen, L. Wang, M. Makihata, H. C. Liu, T. Zhou and X. Zhao, *Science*, 2022, **377**, 517–523.

17 B. Ma, C. Xu, J. Chi, J. Chen, C. Zhao and H. Liu, *Adv. Funct. Mater.*, 2019, **29**, 1901370.

18 C. Zhao, W. Zeng, D. Hu and H. Liu, *IEEE Sens. J.*, 2021, **21**, 15962–15971.

19 J. Xu, C. Zhao, B. Ding, X. Gu, W. Zeng, L. Qiu, H. Yu, Y. Shen and H. Liu, *IEEE Sens. J.*, 2022, **22**, 11526–11534.

20 S. H. Lee, Y. S. Kim, M. K. Yeo, M. Mahmood, N. Zavanelli, C. Chung, J. Y. Heo, Y. Kim, S. S. Jung and W. H. Yeo, *Sci. Adv.*, 2022, **8**, eabo5867.

21 A. Q. Javaid, H. Ashouri, A. Dorier, M. Etemadi, J. A. Heller, S. Roy and O. T. Inan, *IEEE Trans. Biomed. Eng.*, 2017, **64**, 1277–1286.

22 H. Lee, H. Chung, J.-W. Kim and J. Lee, *IEEE Sens. J.*, 2019, **19**, 3861–3870.

23 Y. Ye, Y. Cheng, W. He, M. Hou and Z. Zhang, *IEEE Sens. J.*, 2016, **16**, 7133–7141.

24 B. Park, J. H. Shin, J. Ok, S. Park, W. Jung, C. Jeong, S. Choy, Y. J. Jo and T. I. Kim, *Science*, 2022, **376**, 624–629.

25 C. Wang, H. Wang, B. Wang, H. Miyata, Y. Wang, M. O. G. Nayeem, J. J. Kim, S. Lee, T. Yokota, H. Onodera and T. Someya, *Sci. Adv.*, 2022, **8**, eabo1396.

26 P. Tan, H. Wang, F. Xiao, X. Lu, W. Shang, X. Deng, H. Song, Z. Xu, J. Cao, T. Gan, B. Wang and X. Zhou, *Nat. Commun.*, 2022, **13**, 358.

27 Y. Liu, Y. Cheng, L. Shi, R. Wang and J. Sun, *ACS Appl. Mater. Interfaces*, 2022, **14**, 12812–12823.

28 X. Liu, J. Liu, J. Wang, T. Wang, Y. Jiang, J. Hu, Z. Liu, X. Chen and J. Yu, *ACS Appl. Mater. Interfaces*, 2020, **12**, 5601–5609.

29 A. Galli, C. Narduzzi and G. Giorgi, *IEEE Trans. Instrum. Meas.*, 2018, **67**, 1102–1110.

30 M. A. Motin, C. K. Karmakar and M. Palaniswami, *IEEE J. Biomed. Health. Inform.*, 2018, **22**, 766–774.

31 H. Chung, H. Lee and J. Lee, *IEEE J. Biomed. Health. Inform.*, 2019, **23**, 1595–1606.

32 R. Wang, G. Blackburn, M. Desai, D. Phelan, L. Gillinov, P. Houghtaling and M. Gillinov, *JAMA Cardiol.*, 2017, **2**, 104–106.

33 S. H. Lee, Y.-S. Kim and W.-H. Yeo, *Adv. Healthcare Mater.*, 2021, **10**, 2101400.

34 G. Feiertag, M. Winter, P. Bakardjiev, E. Schröder, C. Siegel, M. Yusufi, P. Iskra and A. Leidl, *Procedia Eng.*, 2011, **25**, 1509–1512.

35 Z. Yi, Z. Liu, W. Li, T. Ruan, X. Chen, J. Liu, B. Yang and W. Zhang, *Adv. Mater.*, 2022, **34**, 2110291.